


Characterization of fibrillar collagen isoforms in infarcted mouse hearts using second harmonic generation imaging: supplement

SUSHANT P. SAHU,¹ QIANGLIN LIU,² ALISHA PRASAD,³ SYED MOHAMMAD ABID HASAN,³ QUN LIU,⁴ MARIA XIMENA BASTIDAS RODRIGUEZ,⁴ ORNA MUKHOPADHYAY,⁵ DAVID BURK,⁶ JOSEPH FRANCIS,⁷ SUPRATIK MUKHOPADHYAY,⁴ XING FU,^{2,8} AND MANAS RANJAN GARTIA^{3,9} 

¹*Department of Chemistry, University of Louisiana at Lafayette, Lafayette, LA 70504, USA*

²*LSU AgCenter, School of Animal Sciences, Louisiana State University, Baton Rouge, LA 70803, USA*

³*Department of Mechanical and Industrial Engineering, Louisiana State University, Baton Rouge, LA 70803, USA*

⁴*Department of Computer Science, Louisiana State University, Baton Rouge, LA 70803, USA*

⁵*Baton Rouge Magnet High School, Baton Rouge, LA 70806, USA*

⁶*Shared Instrumentation Facility and Pennington Biomedical Research Center, Baton Rouge, LA 70808, USA*

⁷*Comparative Biomedical Sciences, School of Veterinary Medicine, Louisiana State University, Baton Rouge, LA 70803, USA*

⁸*xfu1@agcenter.lsu.edu*

⁹*mgartia@lsu.edu*

This supplement published with The Optical Society on 23 December 2020 by The Authors under the terms of the [Creative Commons Attribution 4.0 License](https://creativecommons.org/licenses/by/4.0/) in the format provided by the authors and unedited. Further distribution of this work must maintain attribution to the author(s) and the published article's title, journal citation, and DOI.

Supplement DOI: <https://doi.org/10.6084/m9.figshare.13376897>

Parent Article DOI: <https://doi.org/10.1364/BOE.410347>

Characterization of Fibrillar Collagen Isoforms in the Infarcted Mouse Hearts Using Second Harmonic Generation Imaging: supplemental document

1. Extended Discussion

Collagen is the primary component of the cardiac extracellular matrix (ECM). The three polypeptide alpha chains of the collagen are held together via hydrogen bonding between amide bonds. The individual collagen molecules self-assemble into fibrils of 10-300 nm in width and up to a few hundred microns in length in connective tissues and can further assemble into large bundles or fibers with diameters of ~ 500 nm to several micrometers [1-4]. The three-dimensional organization and structural network of collagens in the extracellular matrix plays a critical role in the proper function of cardiac tissues and organs. Multiple features of the ECM affects mechanical function of the heart, including collagen content [5], types of collagen [6], fiber length and thickness [7], fiber orientation [8], and level of cross-linking [9, 10]. Fibrillar collagens due to their inherent non-centrosymmetric geometry exhibit large nonlinear coefficient originating from ordered tight alignment of large number of polarizable peptide bonds in collagen molecules (1000 amino acids/triple helix) referred as harmonophores along the same direction contributes to amplified SHG signals and is typically governed by strong hyperpolarizability (β) of molecules [2-4]. Indeed, the nonlinear coefficient or related hyperpolarizability for collagen type I ($\beta^{mol,SHG} = (1.7 \pm 0.2) \times 10^{-37} \text{ m}^4 \text{ V}^{-1}$) [11, 12] is determined to be quite competitive, ~ 0.4-0.6 that of commercially available frequency doubling (SHG) non-linear crystals of KDP (potassium di hydrogen phosphate, KH_2PO_4) [13].

SHG is a second order, non-linear optical process, wherein two photons of frequency ω are spatially and temporally overlapped at the sample, to produce a single photon with frequency of 2ω . According to the electric dipole approximation, centrosymmetric or isotropic materials do not produce SHG. This is because the net dipole moment and polarizability of the system become zero due to the random orientations of the probed molecular dipoles [2-4, 14]. When electromagnetic fields interact with a medium, they can induce a material polarization (dipole) “ P ”, which can be expressed as a power series expression as follows:

$$\vec{P} = \alpha^1 E_\omega + \frac{1}{2} \beta^2 E_\omega E_\omega + \frac{1}{6} \beta^3 E_\omega E_\omega E_\omega + \dots \quad (1)$$

Here, α^1 is the polarizability, β^2 is the second-order polarizability (or first-order hyperpolarizability), and β^3 is the third-order polarizability. This polarizability describes the charge oscillation in molecules depending on the strengths of the interacting fields. The SHG signal can be expressed as: $E_{SHG} \propto |P^{(2)}| = \chi^{(2)} E_w E_w$, where $\chi^{(2)}$ is the second order non-linear susceptibility. With $E_{SHG} = \sqrt{I_{SHG}}$, or $I_{SHG} = [\chi^{(2)} E_w E_w]^2$, $\chi^{(2)}$ being proportional to the number density of molecules (N) contributing to SHG and hyperpolarizability (β), $\chi^{(2)} \sim N \beta$. Hence, SHG signal has quadratic dependency ($\text{SHG} \sim N^2$) with the density of collagen molecules [14-16, 40]. Collagen structures showed very strong hyperpolarizability due to its high density, fibrillar non-centrosymmetric structural organization, and associated alignment of repeating peptide bonds ($\beta^{pept} = (2.9 \pm 0.3) \times 10^{-40} \text{ m}^4 \text{ V}^{-1}$) [15] with polarizable electrons. This arises from coherent amplification of radiation fields through constructive interferences by all peptide bonds directed along the collagen triple helix within the interacting laser focal volume. Therefore, SHG signal is a function of concentration and type of organization of collagen. Hence, it is possible to utilize SHG signal modulation for qualitative and quantitative assessment of cardiac fibrosis as shown in this work.

2. Schematic of MI injury model and PSF analysis

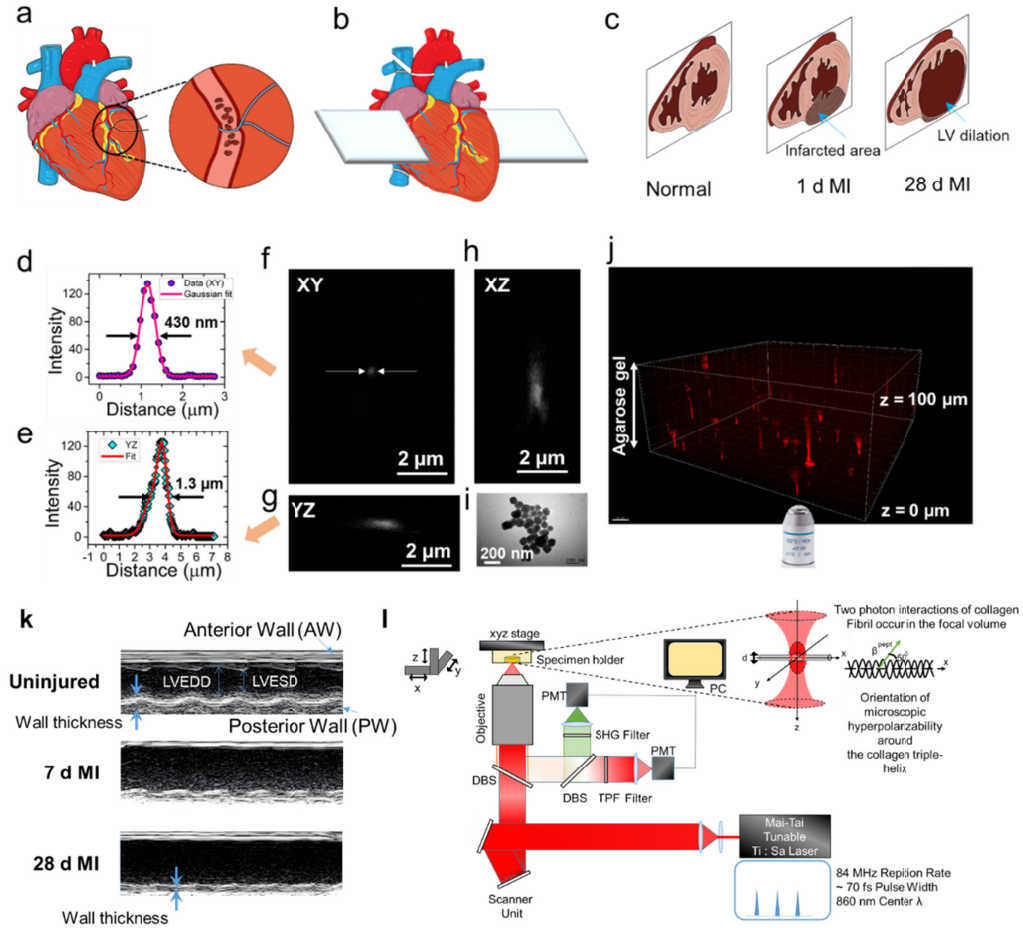


Fig. S1. Schematic representation of MI injury model and characterizing resolution of the two-photon microscope. (a) MI is induced through surgical ligation of the left coronary artery to suppress the blood flow resulting in MI. (b) Extraction and slicing of heart tissue sections for structural characterization and quantification of extracellular matrix (ECM) proteins. (c) The schematic shows the regional remodeling of the heart tissue after MI. It shows the progression of left ventricular (LV) remodeling, infarct expansion, LV wall thinning, ischemic zone dilation, and reparative fibrosis. Assessment of lateral (xy) and depth (xz) resolution of SHG microscopy system using the SHG scattering intensity profile of 100 nm BaTiO₃ bead in (d) xy , (e) yz -plane. Point spread function (PSF) collected from SHG image of the bead in (f) xy , (g) yz , (h) xz -plane. (i) TEM image of the BaTiO₃ beads. (j) 3D scattering images of beads embedded in agarose gel to mimic scattering in tissues. (k) Representative echocardiographic images showing the thinning of left ventricular free wall and dilation of left ventricle after MI. Here, LVEDD: Left Ventricular End Diastolic Diameter; LVESD: Left Ventricular End-Systolic Diameters. (l) Experimental set up of SHG microscope and related instrumentation for imaging collagen. The SHG emission from the tissue collagen is captured with a band-pass SHG filter transmitting 320-435 nm light while two photon fluorescence (TPF) is collected through a narrow range band pass filter from 486-506 nm. 63x, 1.4 NA oil objective was used to obtain the PSF from individual nanoscale beads.

3. ImageJ Analysis Methods

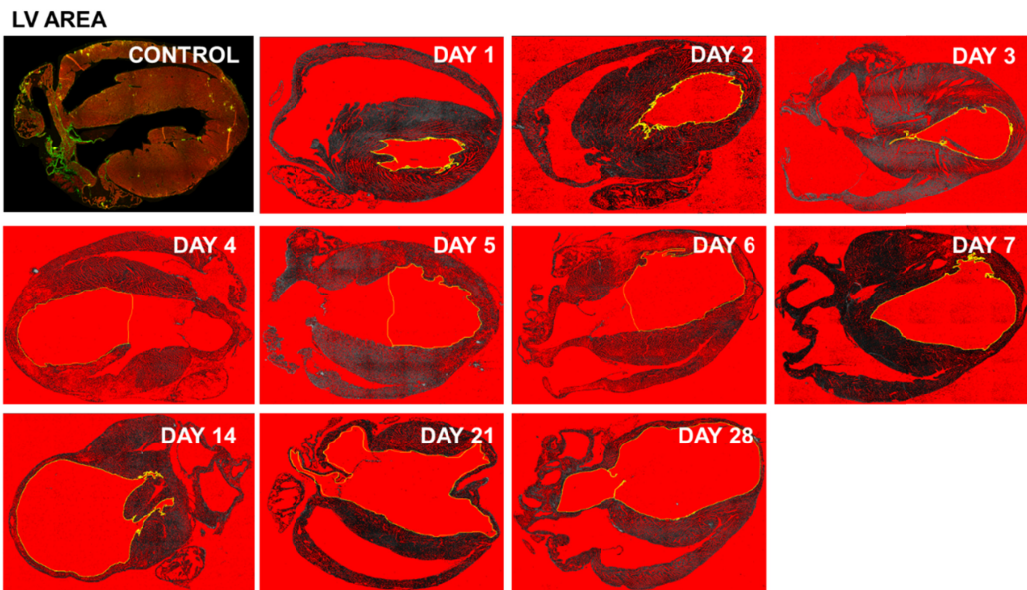


Fig. S2. Image segmentation method implemented in ImageJ to calculate the left ventricular (LV) area. The selected area is shown by yellow line in the images.

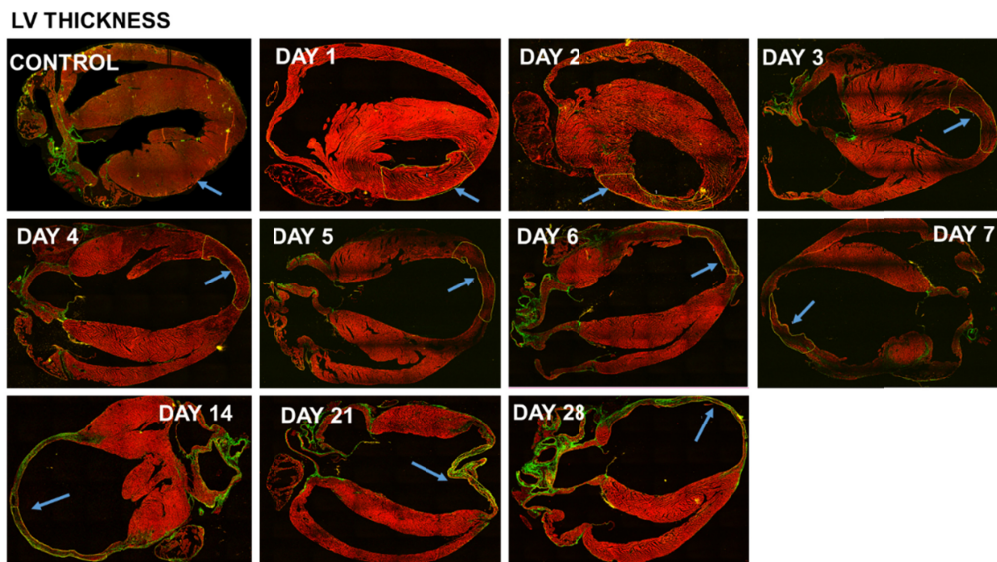
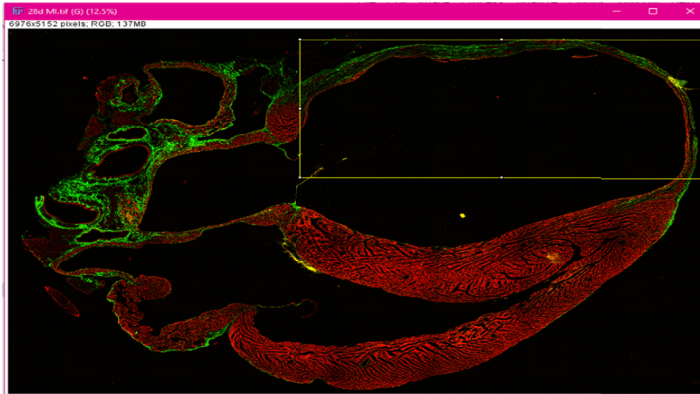


Fig. S3. Image segmentation method implemented in ImageJ to calculate the LV thickness. The blue arrow indicates the segmented LV region (yellow enclosure) used for the analysis. 10x, 0.4 NA air objective was used to collect the SHG from all tissue specimens.

Steps to calculate the collagen contents in SHG images using ImageJ.

Open Image J (<https://imagej.net/Fiji>)

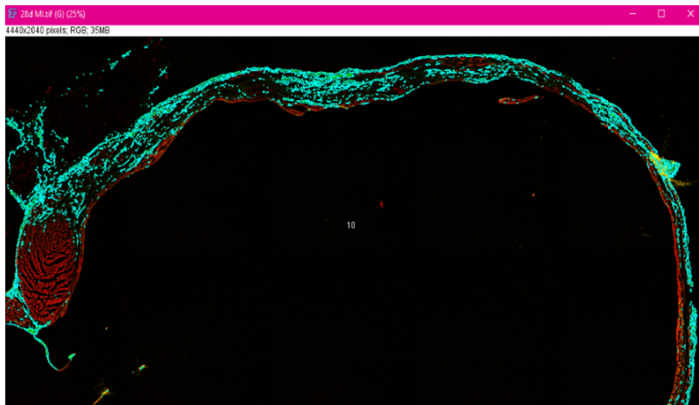
File→Open→Choose File (Image in .TIF/.JPEG/.JPG)



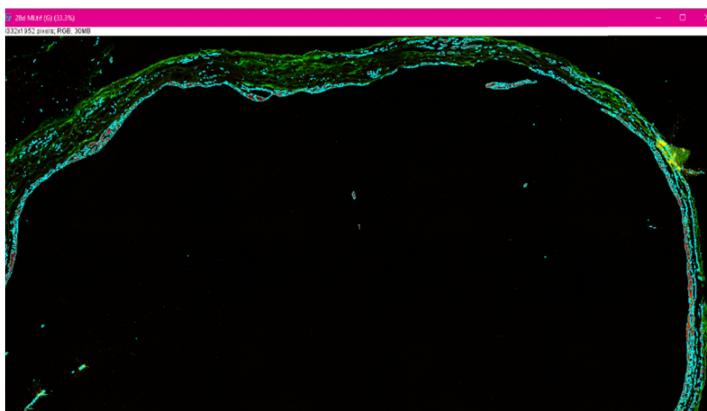
Original Image

Image→Adjust→Threshold→Color Threshold. In the Threshold Dialog Box, Adjust Hue (Select→ Hue as per desired)

Analyze →Select ROI (Region of Interest)



Thresholding, ROI (Fibrosis) Highlighted in Blue



Thresholding, ROI (SHG) Highlighted in Blue

Analyze →Set Measurements (Area, Intensity, Minimum, Maximum etc.)→ Measure

Save as Measurements Recorded as Excel files.

WHOLE TISSUE COLLAGEN & AUTOFLUORESCENCE (GLOBAL)

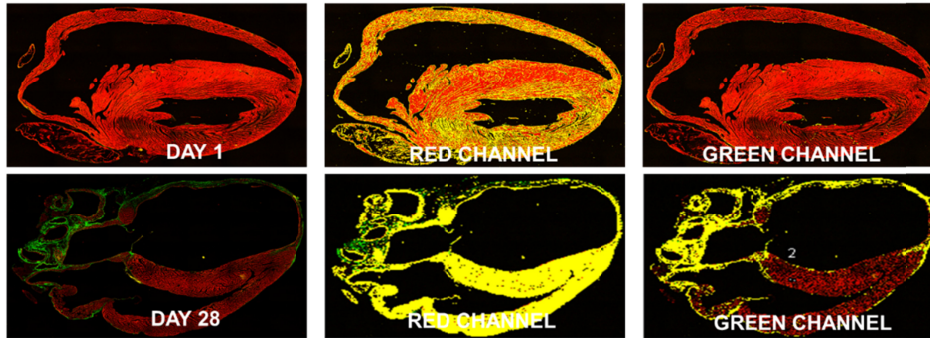


Fig. S4. SHG image analysis implemented in ImageJ using the whole heart tissue section to calculate the collagen content (green channel) and the amount of autofluorescence (red channel). Sample analysis is shown for the tissue collected from MI induced mice on day 1 and day 28. The “matched” pixel selected by the analysis is shown by yellow color for each channel.

LV COLLAGEN & AUTOFLUORESCENCE

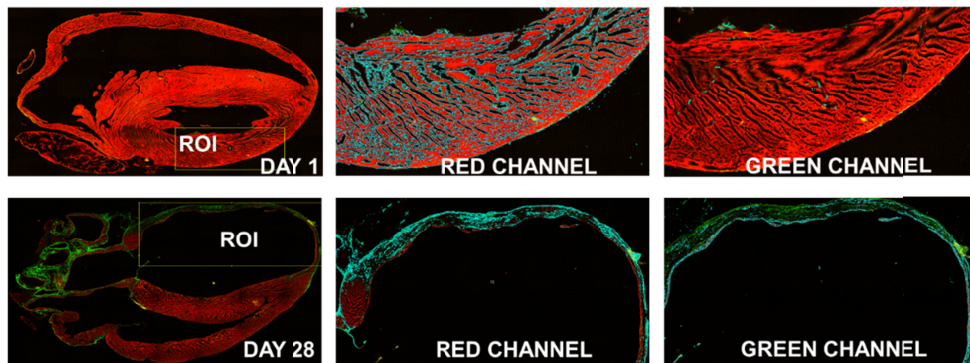


Fig. S5. SHG image analysis implemented in ImageJ using the LV region of the tissue section to calculate the collagen content (Green Channel) and the amount of autofluorescence (Red Channel). Sample analysis is shown for the tissue collected from MI induced mice on day 1 and day 28. The “matched” pixel selected by the analysis is shown by cyan color for each channel.

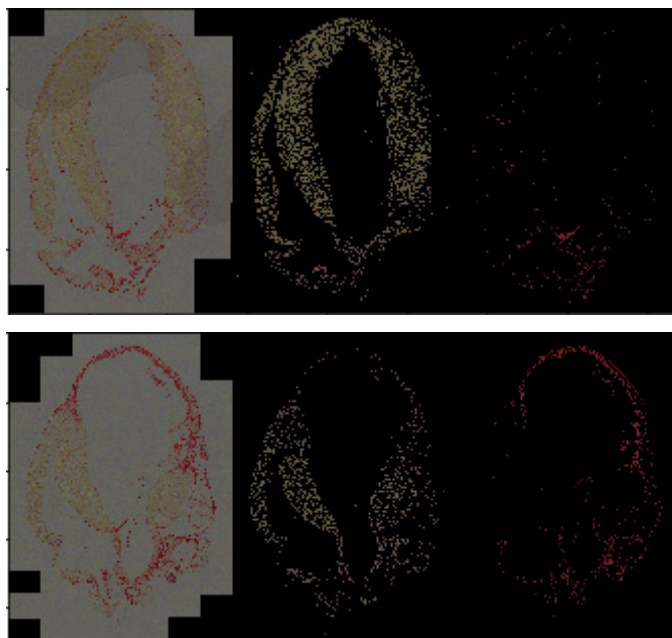


Fig.S6. Image segmentation method implemented for analysis of a representative PSR image for control (top panel) and on day 14 post-MI (bottom panel). The selected pixels for analysis are shown in red.

4. Picrosirius red (PSR) imaging of cardiac tissues

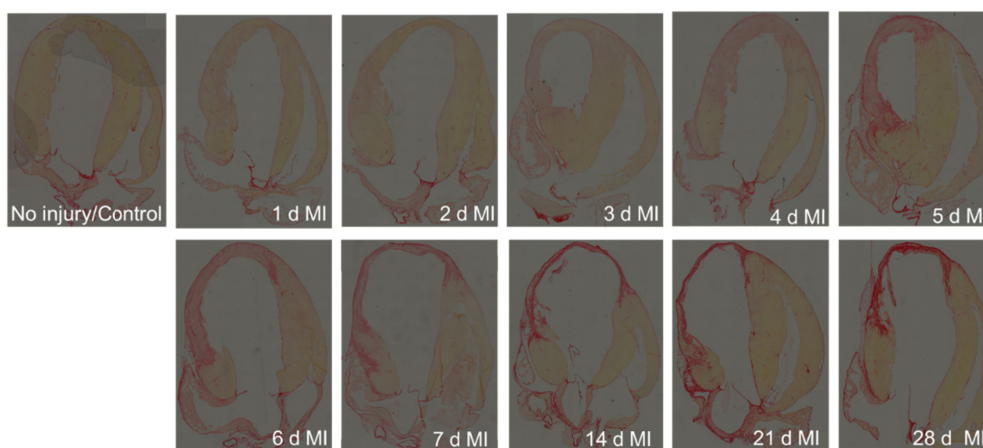


Fig. S7. Representative picrosirius red (PSR) stained heart tissue images under bright field mode using transmitted light microscopy at specified time points post-MI.

5. Polarized light microscopy images of the cardiac tissues

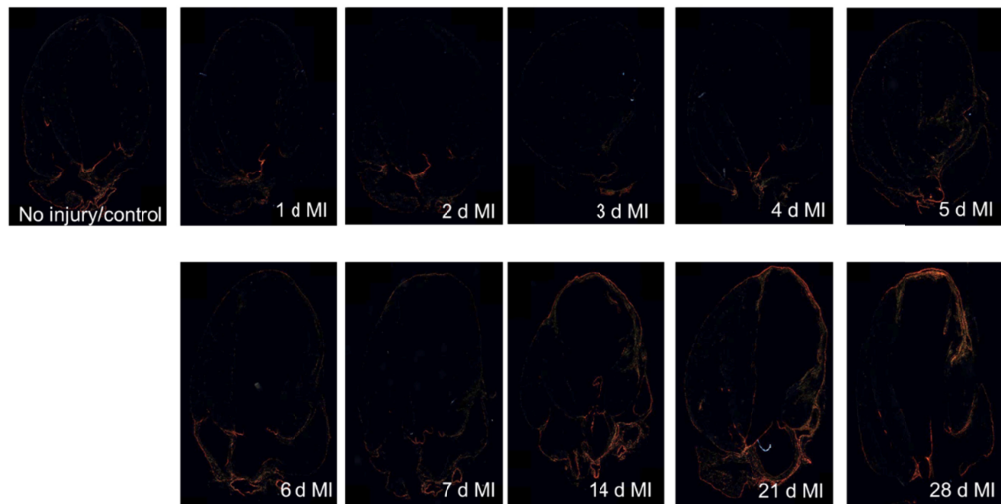


Fig. S8. Representative picosirius red (PSR) stained heart images for PSR-enhanced birefringence detection using polarized light microscopy at indicated time points following MI.

6. Collagen fiber analysis post-MI

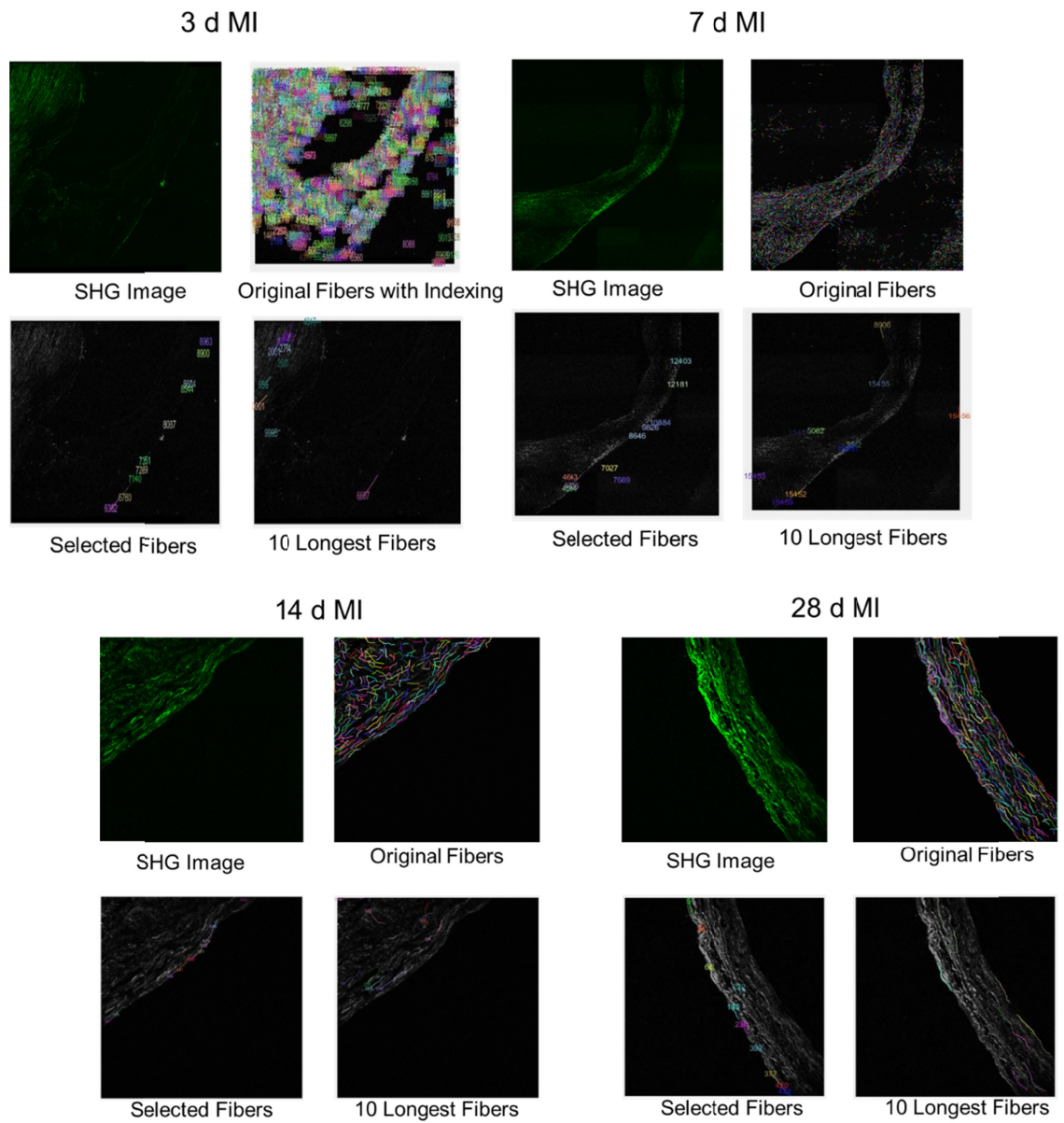


Fig. S9. Collagen fiber analysis of the cardiac tissues post-MI using CT-FIRE program.

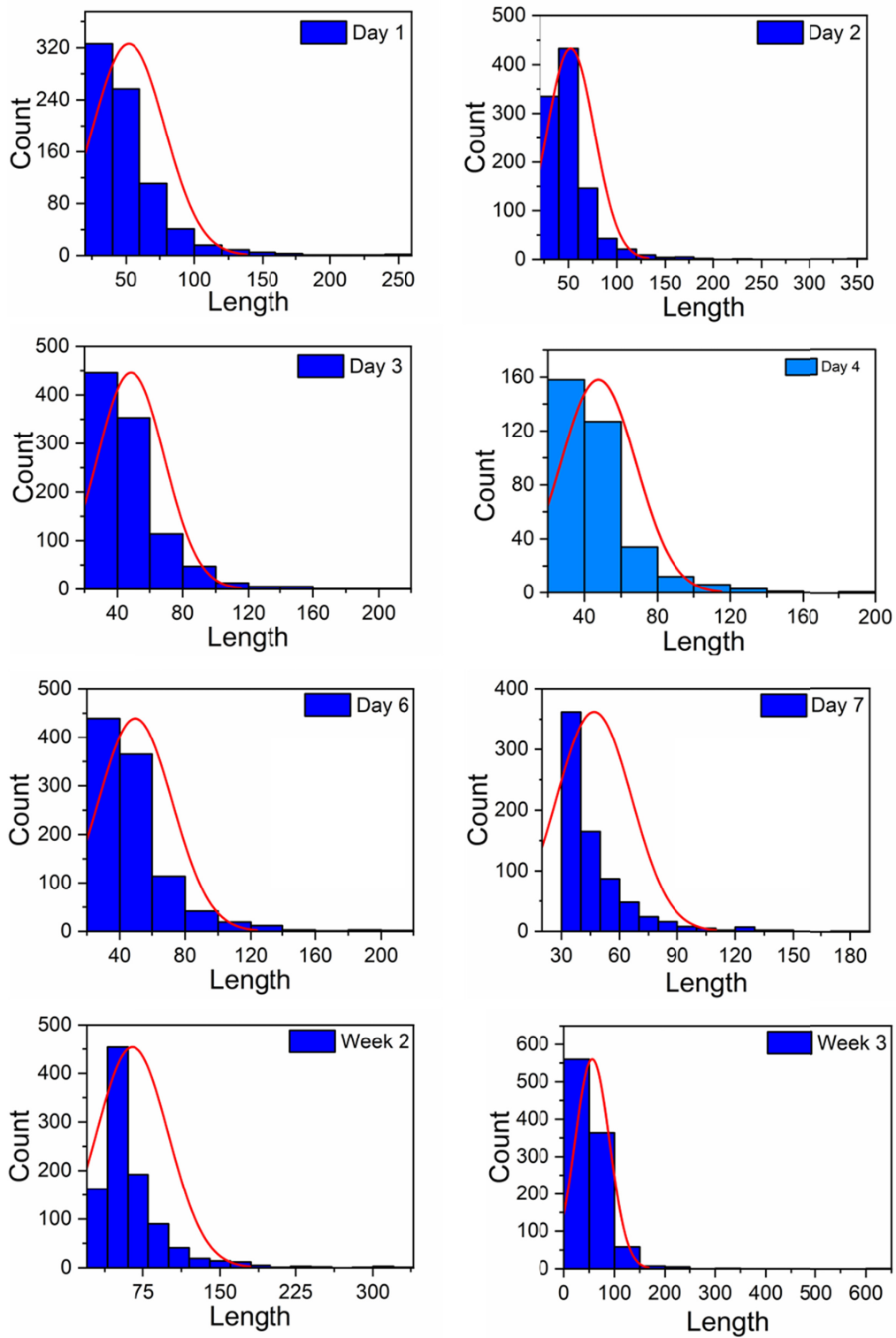


Fig. S10. Distribution of the length (μm) of collagen fibers on different days post-MI.

7. Immunofluorescence imaging of collagen I and III

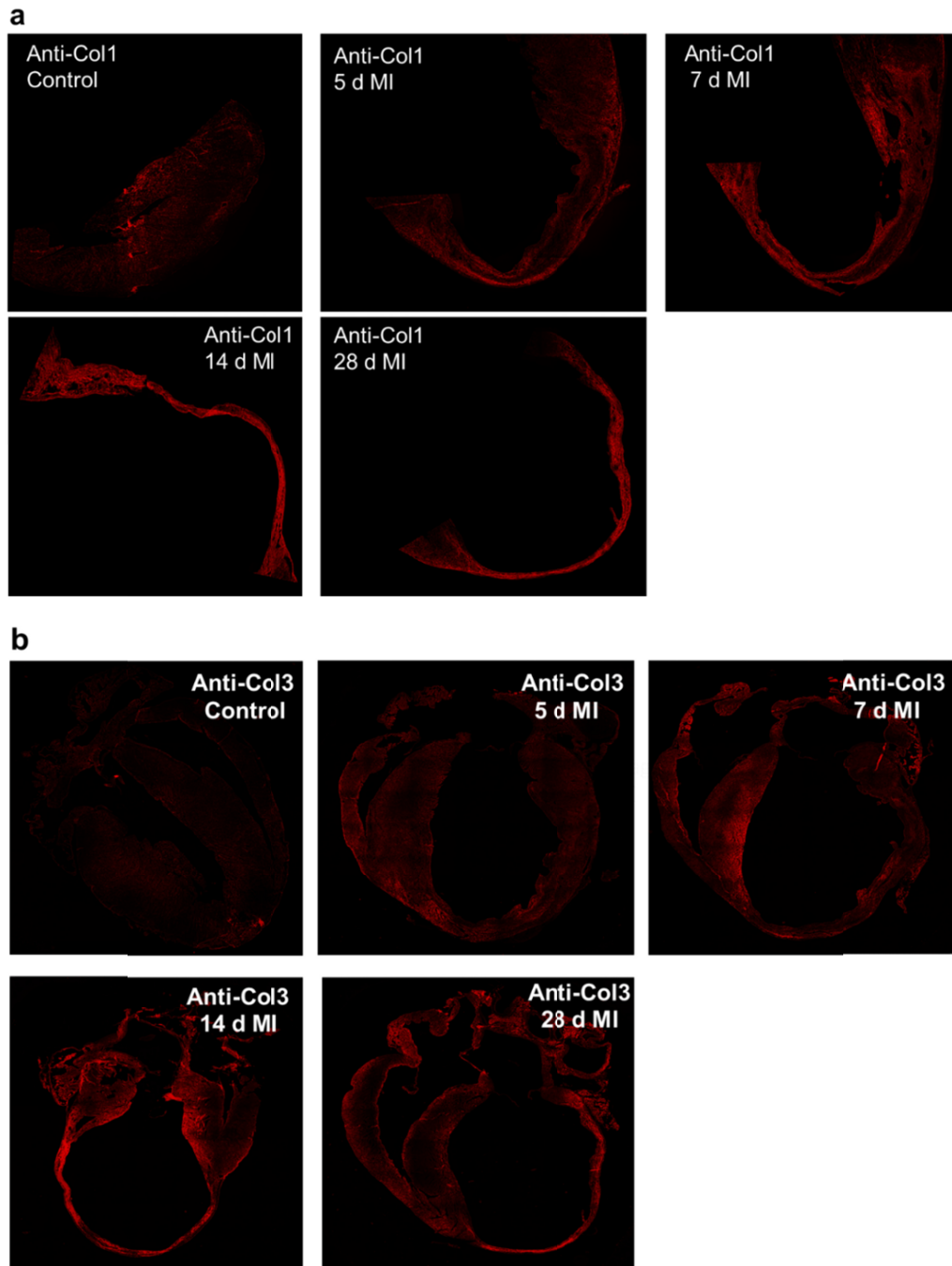
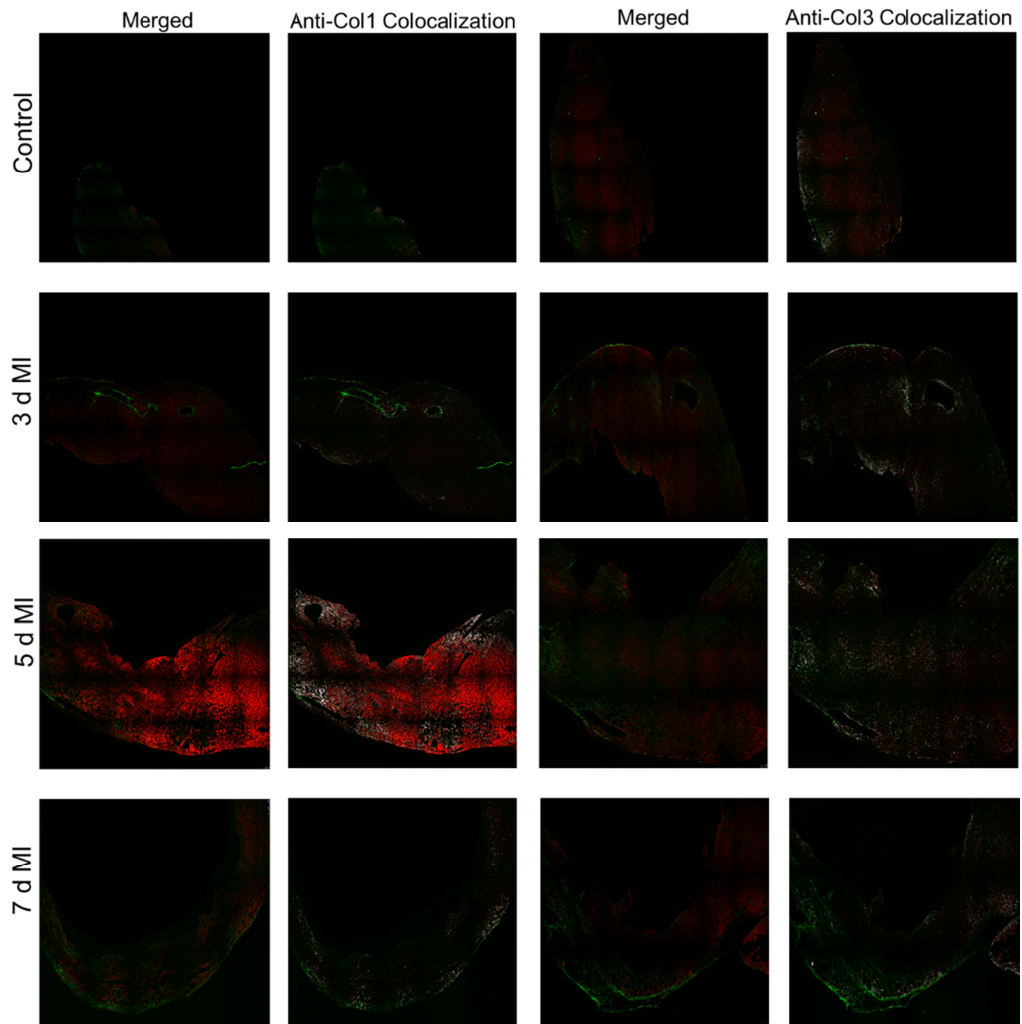


Fig. S11. (a) Immunofluorescence imaging using fluorescently labeled collagen antibodies to highlight collagen isoform distributions, anti-Col1 (Left Ventricle) and (b) anti-Col3 fibers in the infarcted mouse hearts post-MI injury at indicated time points in days.

8. Comparison of SHG and immunofluorescence staining



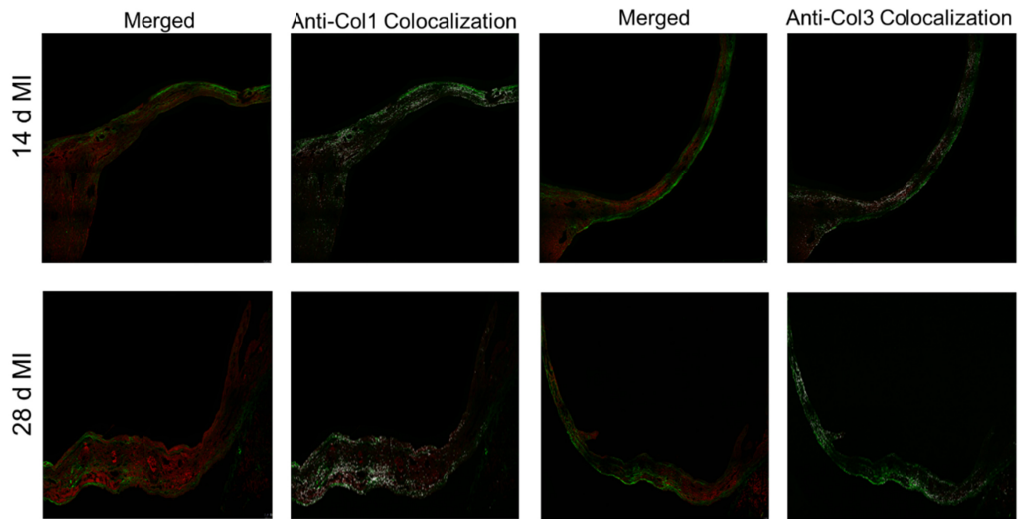


Fig. S12. Nonlinear SHG and immunofluorescence images of Alexa 647 dye labeled anti-Col 1 (Left panels) and anti-Col3 (Right panels) tissue specimens in the selected LV scar zone at different time points in days post-MI in order to determine colocalization extent between SHG and fluorescence from collagens shown by pseudo white colored pixels representing colocalization. 25x, 0.95 NA water objective lens is used to capture the images.

9. Image analysis for the immunofluorescence staining

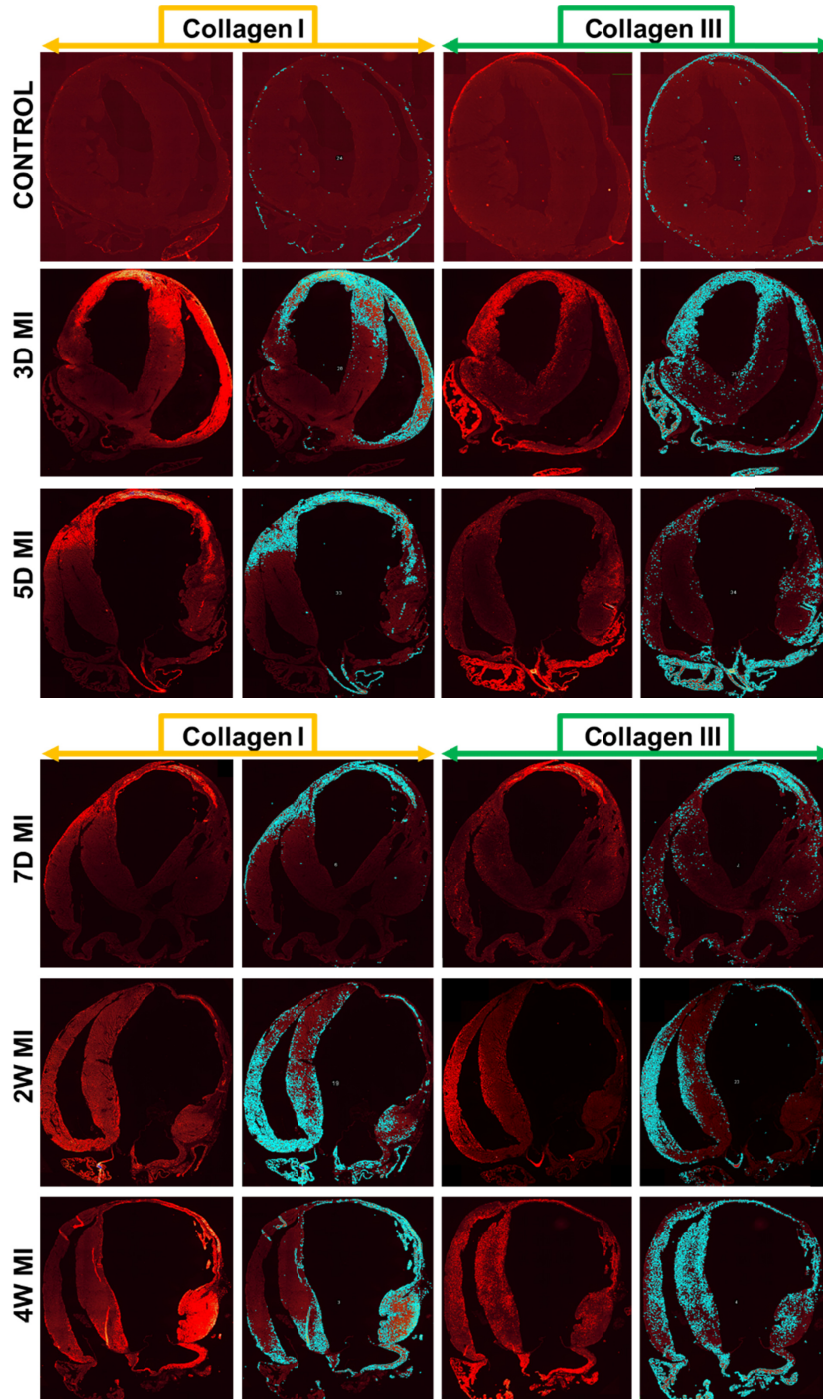


Fig. S13. Image analysis employed in ImageJ for the immunofluorescence antibodies targeting Collagen type I and III in the cardiac tissues.

10. Colocalization analysis for SHG and immunofluorescence data

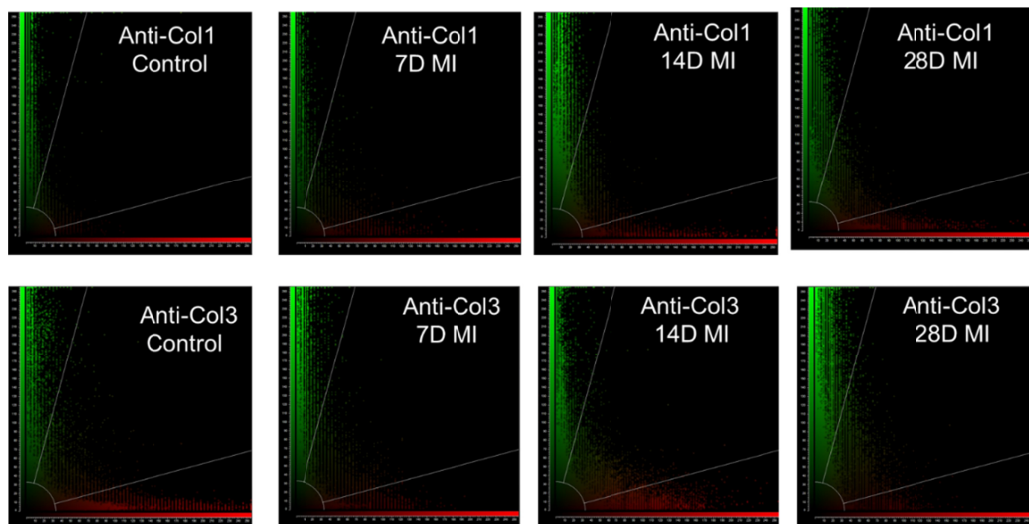


Fig. S14. Selected scatter plots of pixel intensities in SHG channel and Alexa-647 labeled anti-collagen 1 (top panels) and anti-collagen 3 (bottom panels) fluorescence Channel as a function of MI infarction time in days. The intensity of a given pixel in the green channel (SHG) is used as the y-coordinate of the scatter plot and the intensity of the corresponding pixel in the red channel (FL) as the x-coordinate. Scatterplots show the relationship between the signal intensity for two channels of individual SHG and FL images.

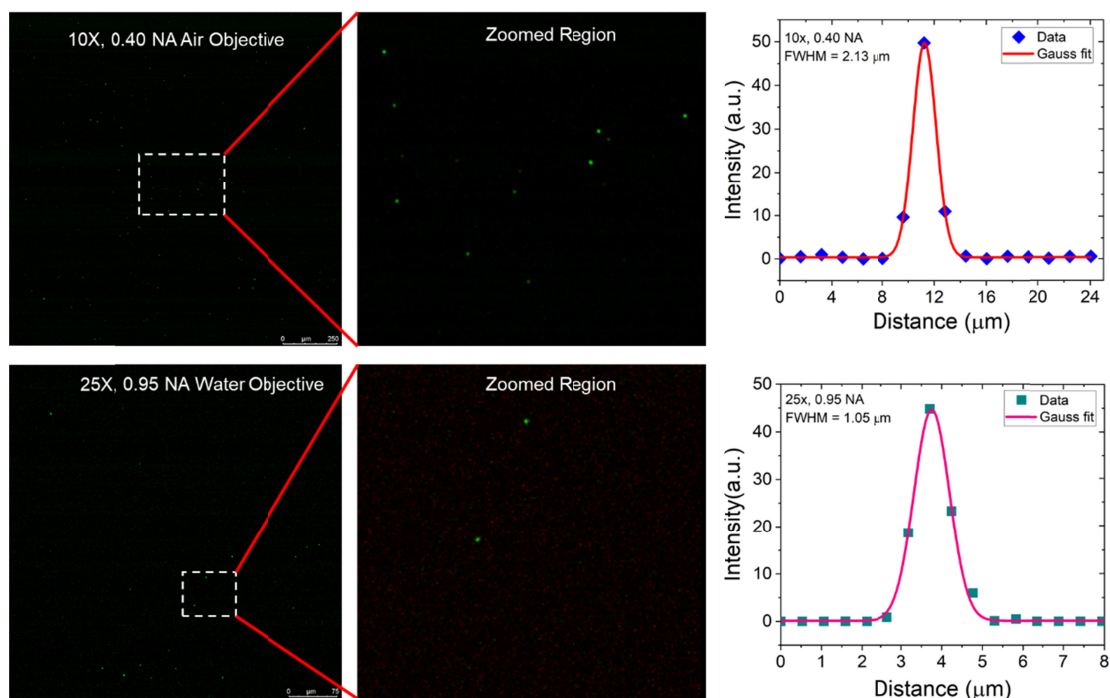


Fig. S15. Experimentally measured lateral point spread function (PSF) afforded by 10X, 0.40 NA (Top panel) and 25X, 0.95 NA (Bottom panel) objectives using sub-diffraction BaTiO₃ nanoparticles.

References

1. M. D. Shoulders and R. T. Raines, "Collagen structure and stability," *Annu. Rev. Biochem.* **78**, 929-958 (2009).
2. X. Chen, O. Nadiarynk, S. Plotnikov, and P. J. Campagnola, "Second harmonic generation microscopy for quantitative analysis of collagen fibrillar structure," *Nat. Protoc.* **7**, 654 (2012).
3. P. Campagnola, "Second harmonic generation imaging microscopy: applications to diseases diagnostics," *Anal. Chem.* **83**, 9, 3224-3231 (2011).
4. L. Mostaço-Guidolin, N. L. Rosin, and T.-L. Hackett, "Imaging collagen in scar tissue: developments in second harmonic generation microscopy for biomedical applications," *Int. J. Mol. Sci.* **18**, 1772 (2017).
5. L. S. Matsubara, B. B. Matsubara, M. P. Okoshi, A. C. Cicogna, and J. S. Janicki, "Alterations in myocardial collagen content affect rat papillary muscle function," *Am. J. Physiol. Heart Circ. Physiol.* **279**, H1534-H1539 (2000).
6. N. Nishikawa, T. Masuyama, K. Yamamoto, Y. Sakata, T. Mano, T. Miwa, M. Sugawara, and M. Hori, "Long-term administration of amlodipine prevents decompensation to diastolic heart failure in hypertensive rats," *J. Am. Coll. Cardiol.* **38**, 1539-1545 (2001).
7. D. MacKenna, S. Vaplon, and A. D. McCulloch, "Microstructural model of perimysial collagen fibers for resting myocardial mechanics during ventricular filling," *Am. J. Physiol. Heart Circ. Physiol.* **273**, H1576-H1586 (1997).
8. S. Thomopoulos, G. M. Fomovsky, P. L. Chandran, and J. W. Holmes, "Collagen fiber alignment does not explain mechanical anisotropy in fibroblast populated collagen gels," *J. Biomech. Eng.* **129** (5), 642-650 (2007).
9. G. R. Norton, J. Tsotetsi, B. Trifunovic, C. Hartford, G. P. Candy, and A. J. Woodiwiss, "Myocardial stiffness is attributed to alterations in cross-linked collagen rather than total collagen or phenotypes in spontaneously hypertensive rats," *Circulation* **96**, 1991-1998 (1997).
10. A. Woodiwiss, O. Tsotetsi, S. Sprott, E. Lancaster, T. Mela, E. Chung, T. Meyer, and G. Norton, "Reduction in myocardial collagen cross-linking parallels left ventricular dilatation in rat models of systolic chamber dysfunction," *Circulation* **103**, 155-160 (2001).

11. A. Deniset-Besseau, J. Duboisset, E. Benichou, F. Hache, P.-F. Brevet, and M.-C. Schanne-Klein, "Measurement of the second-order hyperpolarizability of the collagen triple helix and determination of its physical origin," *J. Phys. Chem. B* **113**, 13437-13445 (2009).
12. S. Bancelin, C. Aimé, I. Gusachenko, L. Kowalczyk, G. Latour, T. Coradin, and M.-C. Schanne-Klein, "Determination of collagen fibril size via absolute measurements of second-harmonic generation signals," *Nat. Comm.* **5**, 1-8 (2014).
13. T. A. Theodossiou, C. Thrasivoulou, C. Ekwobi, and D. L. Becker, "Second harmonic generation confocal microscopy of collagen type I from rat tendon cryosections," *Biophys. J.* **91**, 4665-4677 (2006).
14. R. J. Tran, K. L. Sly, and J. C. Conboy, "Applications of surface second harmonic generation in biological sensing," *Annu. Rev. Anal. Chem.* **10**, 387-414 (2017).
15. J. Duboisset, A. Deniset-Besseau, E. Benichou, I. Russier-Antoine, N. Lascoux, C. Jonin, F. o. Hache, M.-C. Schanne-Klein, and P.-F. o. Brevet, "A bottom-up approach to build the hyperpolarizability of peptides and proteins from their amino acids," *J. Phys. Chem. B* **117**, 9877-9881 (2013).